

Dust formation in winds of long-period variables

V. The influence of micro-physical dust properties in carbon stars

Anja C. Andersen^{1,2}, Susanne Höfner¹, and Rita Gautschy-Loidl³

¹ Department of Astronomy & Space Physics, Uppsala University, P.O.Box 515, SE-751 20 Uppsala, Sweden
e-mail: hoefner@astro.uu.se

² Astronomical Obs., NBIfAFG, Copenhagen University, Juliane Maries Vej 30, DK-2100 Copenhagen, Denmark
e-mail: anja@astro.ku.dk

³ Rüti, Switzerland
e-mail: rita@gautschy.ch

Received 21-10-02; accepted 07-01-03

Abstract. We present self-consistent dynamical models for dust-driven winds of carbon-rich AGB stars. The models are based on the coupled system of frequency-dependent radiation hydrodynamics and time-dependent dust formation. We investigate in detail how the wind properties of the models are influenced by the micro-physical properties of the dust grains that are required by the description of grain formation. The choice of dust parameters is significant for the derived outflow velocities, the degrees of condensation and the resulting mass-loss rates of the models. In the transition region between models with and without mass-loss the choice of micro-physical parameters turns out to be very significant for whether a particular set of stellar parameters will give rise to a dust-driven mass-loss or not. We also calculate near-infrared colors to test how the dust parameters influence the observable properties of the models, however, at this point we do not attempt to fit particular stars.

Key words. hydrodynamics - radiative transfer - stars: mass-loss - stars: atmospheres - stars: carbon - stars: AGB and post-AGB

1. Introduction

Mass loss by dust-driven winds of asymptotic giant branch (AGB) stars is probably one of the major mechanism which recycle material in the Galaxy (e.g. Sedlmayr 1994). Most stars ($M_{\star} \leq 8M_{\odot}$) will eventually become AGB stars and subsequently end their life as white dwarfs surrounded by planetary nebulae.

AGB stars are cool ($T_{\star} < 3500$ K) and luminous (L_{\star} of a few 10^3 to a few $10^4 L_{\odot}$), and a majority of them are pulsating long-period variables (LPVs). The outer layers of many AGB stars provide favorable conditions for the formation of molecules and dust grains. Dust grains play an important role for the heavy mass-loss (up to $\dot{M} \sim 10^{-4} M_{\odot}/\text{yr}$) of these stars by transferring momentum from the radiation to the gas. Pulsation causes an extended atmosphere where the dust is condensing. The dust absorbs the light of the central star and re-radiates it at longer wavelengths in the infrared range ($\lambda > 2\mu\text{m}$). The density of material in the circumstellar envelope may be so large that the star completely disappears in the visual range.

Considerable effort has been put into a theoretical description of the mass-loss of AGB stars. At the end stages of stellar evolution the mass-loss rates become so high that they (and not the nuclear burning rates) determine the stellar evolutionary faith. The goal is to develop a mass-loss description that can be used as input to models of stellar evolution and the chemical evolution of the Galaxy.

This paper is the fifth in our series on dust formation in winds of long-period variables. The previous models presented in Paper I-IV (Dorfi & Höfner 1991; Höfner & Dorfi 1992; Höfner et al. 1995; Höfner & Dorfi 1997) are all based on gray radiative transfer while the models presented here are calculated using frequency dependent radiative transfer for the gas and dust (see Höfner et al. 2002 for details). In this paper we focus on the influence of the micro-physical (i.e. optical and chemical) properties of dust grains on the winds of AGB stars, to determine to what extent the choice of micro-physical parameters affects the general mass-loss predictions.

In Sect. 2 we discuss the hydrodynamical models with emphasis on the treatment of the grain formation. Section 3 describes the different types of amorphous carbon dust

used to test the model dependence on the choice of the micro-physical parameters. In Sect. 4 we present the results and show that the choice of opacity data, the values used for the sticking coefficients and the intrinsic dust density of the material, all affect the mass-loss rates and other wind properties resulting from the models. This has an influence on the calculated synthetic colors which are compared with observations. Conclusions are presented in Sect. 5.

2. The hydrodynamical model

Our spherically symmetric hydrodynamical models predict the mass-loss rates of AGB stars by treating in detail the atmosphere and the circumstellar environment around pulsating long-period variable stars. This is done by solving the coupled system of frequency-dependent radiation hydrodynamics and time-dependent dust formation (cf. Höfner et al. 2002) employing an implicit numerical method and an adaptive grid (for details on the numerical technique see Dorfi & Feuchtinger 1995).

2.1. Hydrodynamics and radiative transfer

In our radiation-hydrodynamical models the stellar and circumstellar envelope are described in terms of separate conservation laws for the dust, the gas and the radiation field. The resulting set of nonlinear partial differential equations consist of:

- Equation of continuity (mass conservation).
- Equation of motion (matter momentum conservation).
- Equation of gas internal energy (matter energy conservation).
- 0. moment of the radiative transfer equation (radiation energy conservation).
- 1. moment of the radiative transfer equation (radiation momentum conservation).
- Moment equations for the dust (grain formation and grain growth).
- Poisson equation (self gravitation).

To this system of nonlinear partial differential equations we add the so-called grid equation which determines the locations of the grid points, depending on some critical physical quantities to be resolved during the computations.

For the dust component only certain moments of the grain size distribution have to be known for a complete description of the circumstellar envelope (more details in Sect. 2.2.1).

In contrast to earlier models in this series the models presented here describe the radiation field by a frequency-dependent treatment of the gas and dust (Höfner 1999; Höfner et al. 2002) based on opacity sampling data of molecular opacities (SCAN data base, Jørgensen 1997) at 51 frequency points between 0.25 and 12.5 μm . Solving the frequency-dependent transfer increases the computation time per time step considerably. To keep the computation

time at a reasonable level, the spatial grid points available in the model are reduced from 500 to 100 compared to the gray models presented in e.g. Höfner & Dorfi (1997).

Basically four stellar parameters are needed as input; the stellar mass (M_\star), the effective temperature (T_{eff}), the luminosity (L_\star) of the star and the gas abundance ratio ($\epsilon_{\text{C}}/\epsilon_{\text{O}}$) of carbon to oxygen. However, to describe the pulsation of the star, two additional parameters are required. Pulsation is simulated by a sinusoidal motion of the inner boundary R_{in} which is located below the stellar photosphere. This variable inner boundary is parameterized by a velocity amplitude (Δu) and a pulsation period (P). The luminosity at the inner boundary is variable and no mass flux is allowed across this boundary (cf. Höfner & Dorfi 1997). As in previous models a perfect gas law with $\gamma = 5/3$ and $\mu = 1.26$ is used as equation of state for reasons of comparability.

The dynamical calculations start from a dust free hydrostatic initial model. The radiative pressure on newly formed dust initiates an outward motion and the expansion is followed by the grid out to around 20–30 R_\star . At this radius the outer boundary is fixed, allowing for outflow. A model evolves for typically 100 years. The model calculation is stopped before a significant depletion of the mass inside the computational domain occurs.

2.2. Grain formation in the models

Dust influences the dynamics and thermodynamics of the stellar atmosphere by its opacity. To calculate this opacity we need to know the amount of dust present. Dust formation proceeds far from equilibrium and it is necessary to use a detailed time-dependent description to determine the degree of condensation and other relevant properties of the grains.

Dust is formed by a series of chemical reactions in which atoms or molecules from the gas phase combine to clusters of increasing size. The molecular composition of the gas phase determines which atoms and molecules are available for the cluster formation and grain growth. Dust formation begins with nucleation of critical clusters followed by growth to macroscopic dust grains.

2.2.1. Grain growth

In our models grain formation is treated by the so-called moment method (Gail & Sedlmayr 1988; Gauger et al. 1990). The moment method describes the time evolution of an ensemble of dust grains of various sizes (including effects due to chemical and thermodynamical non-equilibrium) and requires the nucleation rate as external input.

In the moment method the size of a single dust grain is expressed in terms of the number of monomers (N) contained in the grain. A monomer represents the basic element the grain is built of, i.e. a certain species of atoms or molecules. The ensemble of the grains is described by the

size distribution function $f(N, t)$ representing the number densities of dust particles in dependence of their size N . The number density $f(N, t)$ of dust grains containing N monomers is changed by four processes: creation of grains of size N by growth of smaller dust particles and by destruction of larger ones as well as destruction of grains with N monomers by growth or evaporation (see Gail & Sedlmayr 1988 and Gauger et al. 1990 for details).

As long as the size of the dust grains is small compared to the wavelength of the photons in the relevant frequency region, which is the case for late-type stars, the optical properties of the dust do not depend explicitly on the size spectrum $f(N, t)$ but only on a few moments (K_j) of the grain size distribution function defined by

$$K_j = \sum_{N=N_l}^{\infty} N^{j/d} f(N, t), \quad (1)$$

where d denotes the spatial dimension of the grains ($d = 3$ for spherical particles and 2 for planar structures) and N_l is the lower limit of the grain sizes which may be regarded as macroscopic in the thermodynamical sense. In the work presented here we use the value $d = 3$ (i.e. assume spherical grains) and $N_l = 1000$.

From the moments K_j it is possible to calculate quantities like the total number density of dust grains, the mean grain radius and the fraction of condensible material actually condensed into grains.

Considering grains large enough that their thermodynamical properties do not depend on the grain size and assuming that only molecules with up to a few monomers contribute significantly to the growth process the following set of moment equations can be derived (Gauger et al. 1990)

$$\frac{dK_0}{dt} = \mathcal{J} \quad (2)$$

$$\frac{dK_j}{dt} = \frac{j}{d} \frac{1}{\tau} K_{j-1} + N_l^{j/d} \mathcal{J} \quad (1 \leq j \leq d). \quad (3)$$

Here Eq. (2) determines the grain production rate. The quantity $1/\tau$ is the net growth rate of the dust grains and \mathcal{J} is the net transition rate per volume from cluster sizes $N < N_l$ to $N > N_l$, this can be interpreted as the local current density of clusters flowing up-wards in cluster size space from the region $N \leq N_l$ (Gail & Sedlmayr 1988).

The net growth rate $1/\tau$ contains the number densities of the chemical species which take part in the dust formation process. In our models, the relevant quantities are obtained by assuming chemical equilibrium in the gas phase at the gas temperature T_g

$$\left(\frac{1}{\tau}\right)_{\text{CE}} = \sum_{i=1}^I i A_1 v_{th}(i) \alpha(i) f(i, t) \quad (4)$$

$$\left[1 - \frac{1}{\mathcal{S}^i} \frac{\mathcal{K}_i(T_d)}{\mathcal{K}_i(T_g)} \sqrt{\frac{T_g}{T_d}}\right]$$

$$+ \sum_{i=1}^{I'} i A_1 \sum_{m=1}^{M_i} v_{th}(i, m) \alpha_m^c(i) n_{i, m}$$

$$\left[1 - \frac{1}{\mathcal{S}^i} \frac{\mathcal{K}_{i, m}^r(T_g)}{\mathcal{K}_{i, m}^r(T_d)} \frac{\mathcal{K}_{i, m}(T_d)}{\mathcal{K}_{i, m}(T_g)}\right]$$

where \mathcal{K} denotes the dissociation constant of the molecule of the growth reaction and \mathcal{K}^r is the dissociation constant of the molecule involved in the reverse reaction (see Gauger et al. 1990). $f(i)$ and $n_{i, m}$ are the number densities of the i -mers and the molecules containing i -mers which contribute to the grain growth, respectively. A_1 denotes the (hypothetical) monomer surface area $A_1 = 4\pi a_1^2$ where a_1 is the monomer radius (see Eq. (9)), v_{th} the thermal velocities of the corresponding growth species and α the sticking coefficients. The supersaturation ratio \mathcal{S} is defined by

$$\mathcal{S} = \frac{P_{\text{mon}}}{P_{\text{sat}}(T_d)}, \quad (5)$$

which is the ratio of the actual partial pressure of the monomers in the gas phase to the vapor saturation pressure with respect to the dust temperature T_d . If the thermodynamical conditions allow the formation of dust grains the net transition rate \mathcal{J} is assumed to be equal to the nucleation rate, i.e. the rate at which supercritical (stable) clusters are formed out of the gas phase (see Sect. 2.2.2 for details).

The number densities of the molecules relevant to the dust formation are calculated assuming chemical equilibrium between H, H₂, C, C₂, C₂H and C₂H₂ after the fraction of carbon bound in CO has been subtracted. Nucleation, growth and destruction of dust grains are supposed to proceed by reactions involving C, C₂, C₂H and C₂H₂. The values of the elemental abundances are taken to be solar (Allen 1973) except for the carbon abundance which is considered as a free parameter. The dissociation constants $\mathcal{K}(T)$ have been extracted from the JANAF tables (Stull & Prophet 1971).

2.2.2. Grain nucleation

Nucleation is the first stage of the condensation process whereby a vapor transforms to a solid or liquid. This phase change requires some degree of supersaturation in order to drive the system through the relatively unstable reactive intermediates (clusters) between the atomic or molecular vapor and the macroscopic solid or liquid states. Presently no nucleation rates based on calculations of chemical pathways are available for the astrophysical problem under consideration here. Consequently, the nucleation rate which is a function of temperature, density and supersaturation (\mathcal{S}) for a particular vapor is often calculated by either the classical homogeneous nucleation theory (Becker & Döring 1935; Feder et al. 1966) or by the related scaled homogeneous nucleation theory (Hale 1986).

The classical homogeneous nucleation theory was developed to describe the nucleation of volatile¹ materials

¹ A material that readily evaporates.

such as water, hydrocarbons or alcohols at relatively low levels of supersaturation ($\mathcal{S} \sim 1.1 - 5.0$) and temperatures (~ 300 K). The theory was as such not developed to deal with supersaturated refractory² vapors at high temperatures. The theory describes the formation of critical nuclei in a supersaturated vapor by means of thermodynamic quantities. The essential basic assumption of this approach is that the properties of the clusters in the nucleation regime are given by the extrapolation of the bulk properties even into the domain of very small clusters or the interpolation of thermodynamic properties between those of the molecules and the solid particles. With these assumptions both the thermodynamic functions such as entropy and enthalpy and the rate coefficients describing cluster formation and destruction become simple analytical functions of the cluster size N , which allow a straightforward calculation of the rate of formation of critical clusters.

A fundamental result of classical nucleation theory is the existence of a bottleneck for particle formation. The small unstable clusters which form at random from the gas phase have to grow beyond a certain critical size N_* which corresponds to a maximum in the Gibbs free energy of formation and separates the domain of small unstable clusters from the large thermodynamically stable grains. The rate of grain formation is determined by the transition rate \mathcal{J}_* between both regions. The existence of such a critical cluster size also holds in more realistic theories of cluster formation. However, a review of the available experimental literature by Nuth & Ferguson (1993) shows that no experimental data exists to support the application of classical nucleation theory to the condensation of refractory vapors. Refractory vapors seem to condense out at different supersaturation ratios than volatile materials.

The application of classical homogeneous nucleation theory in astrophysical discussions of grain formation is sharply criticized by Donn & Nuth (1985). There was some hope that scaled nucleation theory (Hale 1986) might be a better way to describe the condensation of refractory vapors. The scaled nucleation theory is a generalization of classical nucleation theory by scaling the relevant parameters to those of the vapor at the critical temperature and pressure and the agreement with experimental data for various molecular fluids was rather good (Martinez et al. 2001). As a result of this success scaled nucleation theory was subsequently applied to selected refractory nucleation data (Hale et al. 1989) with some success. However, comparison materials suggest that refractory materials in general can not be described as accurately (i.e. significant deviations occur for lithium, magnesium and bismuth) as the molecular fluids to which the scaled nucleation theory was originally applied (Nuth & Ferguson 1993). It was shown by Martinez et al. (2001) that the reason for the poor agreement of scaled nucleation theory to certain refractory materials appear to be, at least in part, the result of using an overestimated value for the excess surface en-

tropy for liquid metals. Martinez et al. (2001) conclude that refractory materials, as a class, seem to behave differently than the simple fluids studied in the original work by Hale (1986) and that the use of bulk liquid properties to describe a process involving small metallic clusters is problematic and that there therefore is a serious need for more and better nucleation data for refractory materials.

A better description of the nucleation of small refractory clusters, which are needed as input for the moment method, will most likely have to be guided by experiments. For now we will use the classical nucleation theory for our model calculations. We are aware that in this way we introduce uncertainties to our dust description but with no significant improved theory we find it justified to use classical nucleation theory as a first crude approximation for calculating the nucleation rate \mathcal{J}_* . Once an improved description is derived it will be relatively easy for us to change the description of the nucleation rate in the code.

In the present models the supersaturation ratio \mathcal{S} is defined as the ratio of the partial pressure of carbon atoms in the gas phase divided by the saturated vapor pressure of solid carbon (Eq. (5)). As shown in Gail & Sedlmayr (1988) \mathcal{S} depends on the actual lattice temperature of the N -cluster.

The value $\mathcal{S} = 3$ is adopted following Gail & Sedlmayr (1987b) as the minimum value for grain nucleation to occur. As seen from Fig. 1, where the supersaturation ratio \mathcal{S} and the corresponding nucleation rate \mathcal{J}_* is shown for one of the calculated models, the value of \mathcal{S} is on the order of 100 (or at least much larger than unity) in the zone where the nucleation rate peaks.

3. Amorphous carbon dust

Amorphous carbon particles are considered to be the most common type of dust present in circumstellar envelopes of carbon-rich AGB stars. The infrared spectra of late-type stars generally show a dust emissivity law $Q(\lambda) \sim \lambda^{-\beta}$ with a spectral index of $\beta \sim 1$ (e.g. Campbell et al. 1976; Sopka et al. 1985; Martin & Rogers 1987; Gürtler et al. 1995). A λ^{-1} behavior can be expected in a very disordered material like amorphous carbon (e.g. Huffmann 1988; Jäger et al. 1998). Graphite formation in AGB stars seem unlikely, because of the absence of the narrow band at $11.52 \mu\text{m}$ in the observed spectra and the overall shape of infrared graphite spectra which are proportional to λ^{-2} (e.g. Draine & Lee 1984). This is consistent with physical considerations, predicting the formation of inhomogeneous grains with crystalline cores surrounded by amorphous mantles (Gail & Sedlmayr 1984).

3.1. Optical properties of dust

The formation of the dust grains influences the stellar atmosphere in two ways: In the gas phase chemistry, dust formation results in a depletion of certain elements, which influences the molecular composition of the gas, and consequently the corresponding opacities. On the other hand,

² A material that vaporises only at high temperature.

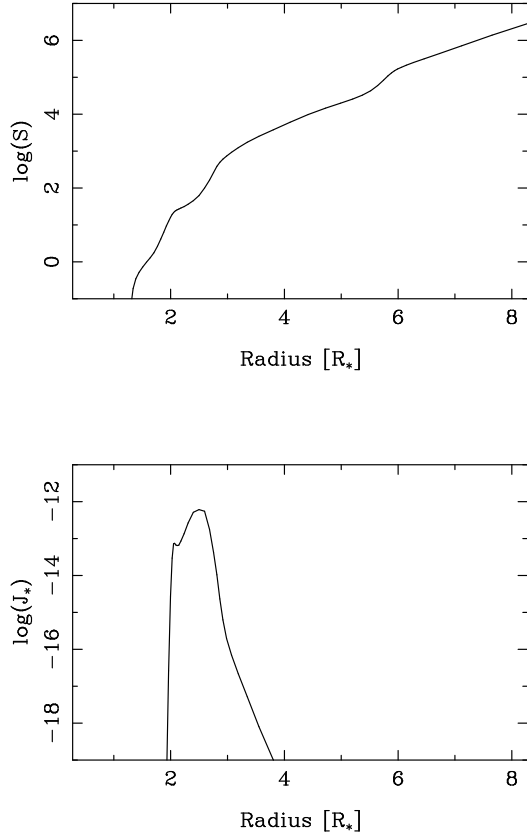


Fig. 1. A snapshot of the supersaturation \mathcal{S} and the nucleation rate \mathcal{J}_* for model l13dj10 ρ 199. The nucleation rate has a sharp maximum around $3R_\odot$ and at this point the supersaturation ratio is around 100.

dust grains have a rather high mass absorption coefficient which often may be comparable to the gas opacity or even exceed it. The total opacity of an ensemble of spherical dust grains can be formulated as

$$\kappa(\lambda) = \int_0^\infty a^2 \pi Q_{\text{ext}}(a, \lambda) n(a) da, \quad (6)$$

where $n(a) da$ is the number density of grains in the grain radius interval between a and $a+da$ and Q_{ext} is the extinction efficiency, i.e. the ratio for the extinction cross section to the geometrical cross section of the grain (Bohren & Huffman 1983). This means that the size distribution function of the dust grains has to be known. However, if the particle size is small compared to the wavelength of the radiation, the small particle limit (SPL), the extinction efficiency Q_{ext} is given by

$$Q'_{\text{ext}}(\lambda) = \frac{Q_{\text{ext}}(\lambda)}{a} = \frac{8\pi}{\lambda} \Im \left(\frac{1-m^2}{2+m^2} \right), \quad (7)$$

where \Im denotes the imaginary part and $m = n + ik$ is the complex refractive index. The dependence of the opacity on wavelength and grain size can therefore be separated into two independent factors

$$\kappa_{\text{ext}}^{\text{SPL}} = Q'_{\text{ext}}(\lambda) \pi \int_0^\infty a^3 n(a) da = \pi a_1^3 Q'_{\text{ext}}(\lambda) K_3. \quad (8)$$

This means that the opacity of the dust particles requires the knowledge of the moment K_3 and the monomer radius a_1 ,

$$a_1 = \left(\frac{3A_{\text{mon}} m_p}{4\pi \rho_{\text{grain}}} \right)^{1/3}, \quad (9)$$

here A_{mon} is the atomic weight of the monomer (for carbon $A_{\text{mon}} = 12.01115$), m_p the proton mass and ρ_{grain} is the intrinsic density of the condensed grain material.

In an astrophysical context, knowledge of the moments K_i for $i = 1, 2, 3$ is needed if the extinction coefficient is required and additionally the moments with $i = 4, 5, 6$ if both absorption and scattering are required separately because the scattering coefficient $\kappa_{\text{sca}}(\lambda)$ depends on K_6 (Gail & Sedlmayr 1984).

The photospheric spectral energy distribution of AGB stars has its maximum around wavelengths of $1 \mu\text{m}$ (with a sharp decline of the stellar flux toward shorter wavelengths), and both observations and theoretical arguments indicate that typical grain sizes in these stars are much smaller than $1 \mu\text{m}$. Thus, the limit of particles being small compared to the wavelength is valid for a major fraction of the spectrum. We therefore do not need to specify details about the size distribution of the grains to calculate the grain opacities required for model atmospheres. However, it may still be necessary to know properties like the size distribution and shapes of the grains to compute detailed synthetic spectra at very short wavelengths. The complex refractive index of the material as a function of wavelength can be determined from laboratory measurements.

3.2. Laboratory measurements of amorphous carbon

Due to the nature of amorphous carbon dust materials they span a broad range of micro-physical properties. In the models presented here we have used three different laboratory measurements (referred to as *Jäger 1000*, *Jäger 400* and *Rouleau*, see Table 1) to describe the opacity of the dust grains formed in the circumstellar envelope.

The data by Jäger et al. (1998) are produced by pyrolyzing cellulose materials at different temperatures. The materials are characterized in exemplary detail. In this study we have used the data synthesized at 400°C and 1000°C . The two materials differ in the bonding, where the *Jäger400* material has more single bonds (the carbon atoms are mainly sp^3 hybridized) while the *Jäger1000* material has more double bonds (the carbon atoms are mainly sp^2 hybridized). Reflectance spectra were obtained of the samples and from these the complex refractive index (m) was derived by the Lorentz oscillator method (see e.g. Bohren & Huffman 1983, Chap. 9).

Rouleau & Martin (1991) produced synthetic optical constants (n and k ; $m = n + ik$) based on measurement of sub-micron amorphous carbon particles by Bussoletti et al. (1987). The particles were produced by striking an arc between two amorphous carbon electrodes in a controlled Ar atmosphere.

Table 1. List of the different dust opacities used.

Reference	Material name	ρ_{grain} (g/cm ³)	sp^2 %	Designation in this paper	Comments
Jäger et al. (1998)	cel400	1.435	67	<i>Jäger 400</i>	completely amorphous
Jäger et al. (1998)	cel1000	1.988	80	<i>Jäger 1000</i>	contains graphite (2 nm) crystallites
Rouleau & Martin (1991)	AC2	1.85	-	<i>Rouleau</i>	

3.3. Grain equilibrium temperature

The presence of dust grains influences both the momentum and the energy balance of the atmosphere. We assume complete momentum coupling of gas and dust, which means that the momentum gained by the dust from the radiation field is directly transferred to the gas. On the other hand, the transfer of internal energy between gas and dust is negligible compared to the interaction of each component with the radiation field (cf. Gauger et al. 1990). We therefore assume that the grain temperature is given by the condition of radiative equilibrium

$$\chi_J J - \chi_S S_d = 0 \Rightarrow T_d = \left(\frac{\chi_J}{\chi_S} \right)^{\frac{1}{4}} T_r \quad (10)$$

where the source function is equal to the Planck function $S_d = B(T_d)$. The frequency-integrated dust opacities are defined by

$$\chi_J = \frac{\int_{\nu} \chi_{\nu} J_{\nu} d\nu}{\int J_{\nu} d\nu} \quad (11)$$

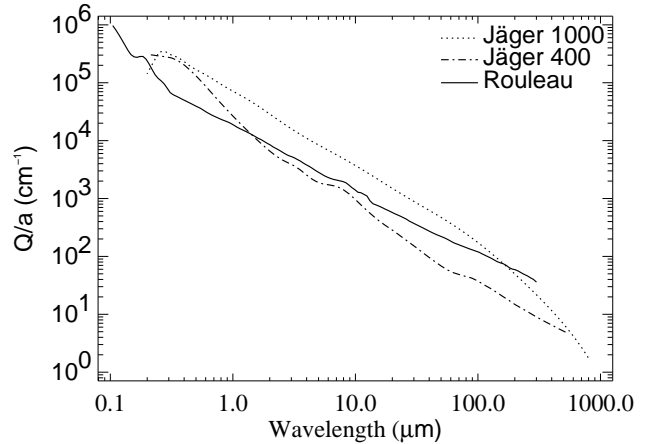
$$\begin{aligned} \chi_S &= \frac{\int_{\nu} \chi_{\nu} S_{\nu} d\nu}{\int S_{\nu} d\nu} = \frac{\int_{\nu} \chi_{\nu} B_{\nu}(T_d) d\nu}{\int B_{\nu}(T_d) d\nu} \\ &= \frac{\int_{\nu} \chi_{\nu} B_{\nu}(T_d) d\nu}{B(T_d)} \end{aligned} \quad (12)$$

where J_{ν} is the radiation energy density, and the radiation temperature $T_r = (J\pi/\sigma)^{1/4}$.

For a gray opacity we would obtain $\chi_J \equiv \chi_S$ for the opacities and the temperatures $T_d \equiv T_r$ as in previous models. Using frequency-dependent radiative transfer the opacities χ_J and χ_S differ. For the data shown in Fig. 2, the absorption coefficients decrease with increasing wavelength in the infrared region of the spectrum, leading to $T_d > T_r$ for all data sets shown. The difference between T_d and T_r becomes larger with an increasing slope of $Q'_{\text{ext}}(\lambda)$ and the difference may reach several 10^2 K in the dust formation zone (Höfner et al. 2002). In other words, the steeper the dependence on wavelength, the larger the difference between the equilibrium grain temperature and the radiation temperature. Therefore, the steeper slope of *Jäger 400* data results in a relatively high grain temperature compared to *Jäger 1000* and *Rouleau*.

4. Results

One of the main reasons for the huge mass-loss of AGB stars seems to be the presence of newly formed dust grains. The strong shock waves in the stellar atmosphere cause

**Fig. 2.** Wavelength dependence of the dust absorption efficiency Q'_{ext} (see Table 1 for dust annotation).

a levitation of the outer layers. The cool and relatively dense environment which results from the levitation provides favorable conditions for the formation of molecules and grains. Due to its high opacity and the resulting radiative pressure, the dust has a strong influence on the structure of the atmosphere and the wind properties.

4.1. Influence of the dust extinction coefficient

The influence of the dust extinction coefficient on the winds of the dynamical models is shown in Table 2 and Fig. 3. The models depend on the choice of laboratory measurements of $Q'_{\text{ext}}(\lambda)$ as already shown for gray models in Andersen et al. (1999). In contrast to the gray models, for the frequency-dependent models both the absolute value and the slope of the dust opacity data as a function of λ become relevant. The absolute value of the grain opacities mainly affects the terminal velocity of the winds, while the slope has significant influence on the grain temperature as discussed in Sect. 3.3. In the models where the *Jäger 400* data is used for the opacity of the grains, the slope of the extinction efficiency as a function of λ dictates a high grain temperature which prevents dust formation for the chosen stellar parameters. Models with identical stellar parameters using *Jäger 1000* and *Rouleau* data on the other hand develop dust-driven winds.

Figure 3 and Table 2 show that it is not possible to distinguish from near infrared photometry alone between the different models, since the hotter model using the

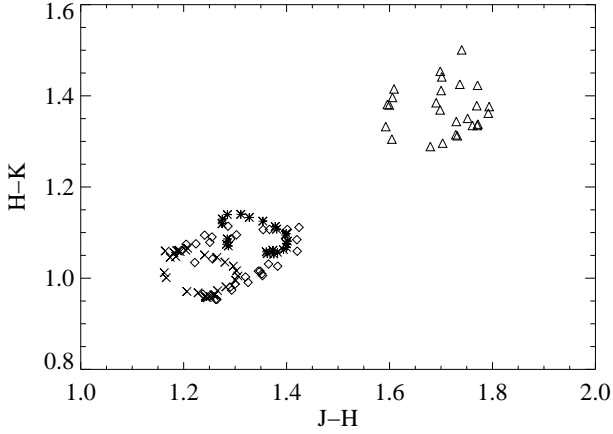


Fig. 3. The colors (J–H) vs. (H–K) of the four models l13dj10ρ199 (\diamond), l10dj10ρ199 (\triangle), l13drouρ185 (\times) and l10drouρ185 ($*$). There are two differences between the two sets of models. (1) The assumed value of the luminosity (L_*) and corresponding effective temperature (T_*), and (2) the dust opacity data used (*Jäger 1000* and *Rouleau*). All other model values are kept constant. See Table 2 for details.

Jäger 1000 opacity data has similar colors as the cooler model using the optical properties from the *Rouleau* data. This is a consequence of the fact that these two models have circumstellar envelopes with comparable optical depth at these wavelengths as can be demonstrated by the following rough estimate; the optical depth of a given layer $d\tau$ can be expressed in terms of the extinction coefficient, the local degree of condensation f_c , mass-loss rate and flow velocity by

$$\begin{aligned} d\tau = \kappa dr &= \pi a_1^3 Q'_{\text{ext}}(\lambda) K_3(r) dr \\ &\propto a_1^3 Q'_{\text{ext}} f_c \rho_{\text{gas}} dr \\ &\propto a_1^3 Q'_{\text{ext}} f_c \frac{\dot{M}}{u} \frac{1}{r^2} dr \end{aligned} \quad (13)$$

where we have used Eq. (8), $K_3 \propto f_c \rho_{\text{gas}}$ and $\rho_{\text{gas}} = \dot{M}/4\pi r^2 u$ to replace the gas density ρ_{gas} . To estimate the relative optical depths of the circumstellar envelopes of different models we assume that we can replace $f_c \dot{M}/u$ by the time-averaged values $\langle f_c \rangle \dot{M}/\langle u \rangle$ at the outer boundary. For models l13dj10ρ199 and l10drouρ185 the differences in mass-loss rate, degree of condensation and outflow velocity as well as the extinction efficiency and the monomer radius compensate each other in such a way that the quantity $a_1^3 Q'_{\text{ext}} \langle f_c \rangle \dot{M}/\langle u \rangle$ is comparable for both models while the value for l10dj10ρ199 differs by about a factor of two. Although it is impossible to distinguish the models l13dj10ρ199 and l10drouρ185 by their near infrared colors alone it would be possible to do this by a combination of photometry and high-resolution spectroscopy due to their significantly different outflow velocities (of about a factor of four).

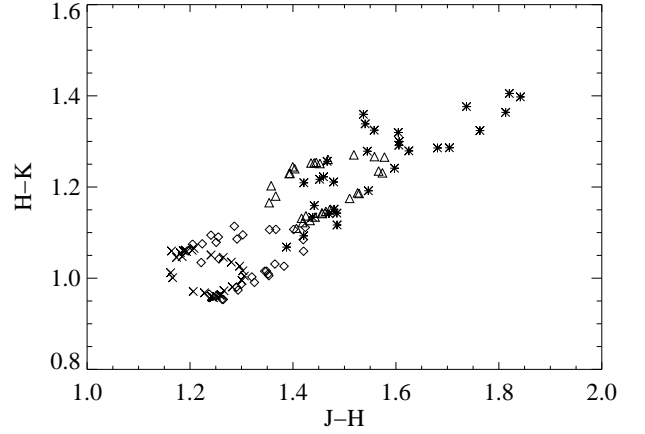


Fig. 4. The colors (J–H) vs. (H–K) for the four models l13dj10ρ199 (\diamond), l13dj10ρ225 ($*$), l13drouρ185 (\times) and l13drouρ225 (\triangle). We see the results for two different opacity data (*Jäger 1000* and *Rouleau*). Two different models for each opacity data are shown. The difference between the two models with the same opacity is the assumed value of the intrinsic density (ρ_{grain}) of the dust material formed in the model. The values correspond to the one determined in the laboratory for the material and the value for graphite (2.25 g/cm^3) which was used in previous models. See Table 3 for details.

4.2. Influence of the intrinsic dust density

When the moment method was developed by Gail & Sedlmayr (1988) the intrinsic density for the amorphous carbon material used in that generation of models (Maron 1990) was not known. The value of graphite (2.25 g/cm^3) was therefore assumed. This value was later used in most existing models based on the moment method (e.g. Fleischer et al. 1992; Höfner & Dorfi 1997).

In the previous section we have described models which use optical properties represented by three different amorphous carbon materials for which the intrinsic densities have been measured in the laboratory. Here, we compare them with three models where the same optical properties were used but where we assumed the higher value for the intrinsic density of graphite instead of the measured value of the material (while keeping all other parameters constant).

The result of using the higher density of graphite instead of the correct values can be seen in Table 3 and Fig. 4. Figure 4 demonstrate that the models become much redder when the intrinsic density of graphite is used instead of the respective values for amorphous carbon. The large increase in the mean degree of condensation $\langle f_c \rangle$ at the outer boundary implies that more dust is formed. This results in an increased radiation pressure on the dust grains and the models therefore show a higher mean velocity $\langle u \rangle$ at the outer boundary. At the same time the mass-loss rates increases so that $a_1^3 \langle f_c \rangle \dot{M}/\langle u \rangle$, which is a measure of the optical depth of the envelope, is significantly

Table 2. Influence of the extinction efficiency of the dust. *Model parameters:* $M_\star = 1.0 M_\odot$, sticking coefficient $\alpha_C = 0.37$, $\alpha_{C_2} = 0.34$, $\alpha_{C_2H} = 0.34$ and $\alpha_{C_2H_2} = 0.34$, $\varepsilon_C/\varepsilon_O = 1.4$, period $P = 650$ d, piston velocity $\Delta u_p = 4$ km/s, luminosity L_\star , temperature T_\star , radius R_\star , dust opacity data κ_{dust} , intrinsic dust density ρ_{grain} ; *Results:* Mass loss rate \dot{M} , mean velocity at the outer boundary $\langle u \rangle$, mean degree of condensation at the outer boundary $\langle f_c \rangle$.

Model	L_\star [L_\odot]	T_\star [K]	R_\star [R_\odot]	κ_{dust}	ρ_{grain} [g/cm ³]	\dot{M} [M_\odot /yr]	$\langle u \rangle$ [km/s]	$\langle f_c \rangle$	Symbol in Fig. 3
l13dj10 ρ 199	13000	2700	521	<i>Jäger 1000</i>	1.99	$5.6 \cdot 10^{-6}$	15	0.05	\diamond
l13drou ρ 185	13000	2700	521	<i>Rouleau</i>	1.85	$4.9 \cdot 10^{-6}$	7.4	0.10	\times
l13dj04 ρ 144	13000	2700	521	<i>Jäger 400</i>	1.44	-	-	-	-
l10dj10 ρ 199	10000	2600	493	<i>Jäger 1000</i>	1.99	$7.0 \cdot 10^{-6}$	16	0.10	\triangle
l10drou ρ 185	10000	2600	493	<i>Rouleau</i>	1.85	$2.3 \cdot 10^{-6}$	3.6	0.12	*
l10dj04 ρ 144	10000	2600	493	<i>Jäger 400</i>	1.44	-	-	-	-

Table 3. Influence of the intrinsic density of the dust. *Model parameters:* Same as Table 2.

Model	L_\star [L_\odot]	T_\star [K]	κ_{dust} g/cm ³	ρ_{grain} [M $_C$ /yr]	\dot{M} [km/s]	$\langle u \rangle$	$\langle f_c \rangle$	Symbol in Fig. 4
l13dj10 ρ 199	13000	2700	<i>Jäger 1000</i>	1.99	$5.6 \cdot 10^{-6}$	15	0.05	\diamond
l13dj10 ρ 225	13000	2700	<i>Jäger1000</i>	2.25	$7.3 \cdot 10^{-6}$	21	0.11	*
l13drou ρ 185	13000	2700	<i>Rouleau</i>	1.85	$4.9 \cdot 10^{-6}$	7.4	0.10	\times
l13drou ρ 225	13000	2700	<i>Rouleau</i>	2.25	$8.2 \cdot 10^{-6}$	18	0.31	\triangle
l13dj04 ρ 144	13000	2700	<i>Jäger400</i>	1.44	-	-	-	-
l13dj04 ρ 225	13000	2700	<i>Jäger400</i>	2.25	$2.1 \cdot 10^{-8}$	1.38	0.13	-

Table 4. Influence of the sticking coefficient for the dust formation. *Model parameters:* Same as Table 2 except for the sticking coefficients: α_C , α_{C_2} , α_{C_2H} and $\alpha_{C_2H_2}$, dust opacity $\kappa_{\text{dust}} = \text{Rouleau}$, and the intrinsic dust density $\rho_{\text{grain}} = 1.85$ g/cm³ for all models.

Model	L_\star [L_\odot]	T_\star [K]	α_C	α_{C_2}	α_{C_2H}	$\alpha_{C_2H_2}$	\dot{M} [M_\odot /yr]	$\langle u \rangle$ [km/s]	$\langle f_c \rangle$	Symbol in Fig. 5
l13drou ρ 185	13000	2700	0.37	0.34	0.34	0.34	$4.9 \cdot 10^{-6}$	7.4	0.10	*
l13drou ρ 185 α 02	13000	2700	0.20	0.20	0.20	0.20	$3.4 \cdot 10^{-6}$	3.9	0.09	-
l13drou ρ 185 α 05	13000	2700	0.50	0.50	0.50	0.50	$5.8 \cdot 10^{-6}$	11	0.12	-
l13drou ρ 185 α 10	13000	2700	1.00	1.00	1.00	1.00	$7.0 \cdot 10^{-6}$	17	0.22	\triangle
l10drou ρ 185	10000	2600	0.37	0.34	0.34	0.34	$2.3 \cdot 10^{-6}$	3.6	0.12	-
l10drou ρ 185 α 10	10000	2600	1.00	1.00	1.00	1.00	$7.0 \cdot 10^{-6}$	12	0.23	-

higher for both models using the density of graphite compared to the respective models with the consistent dust densities.

Even a small increase of about 10% in the density of the dust material (as it is the case from model l13dj10 ρ 199 to l13dj10 ρ 225) results in a doubling of the degree of condensation and a substantial increase of the outflow velocity $\langle u \rangle$ and the mass-loss rate. For the models l13drou ρ 185 and l13drou ρ 225 where the difference in the value used for the intrinsic dust density is about 20%, the estimated mass-loss rates differ by almost a factor of two. For the models using the *Jäger 400* material (l13dj04 ρ 144 and l13dj04 ρ 225), where the difference is almost 40%, using the measured material value instead of the higher value for graphite results in a model that will not develop a wind at all.

The intrinsic dust density of the dust material ρ_{grain} is so significant for the obtained results because when it is

increased the monomer radius a_1 decreases (see Eq. (9)). This influences both the grain growth and the dust opacity. The net growth rate $1/\tau$ and the opacity κ dependent on the monomer radius as $1/\tau \propto a_1^2$ (through the monomer surface A_1) and $\kappa \propto a_1^3$, respectively. A reduction of a_1 decreases the dust mass absorption coefficient stronger than the growth rate, leading both to a slower acceleration and a more efficient growth of the grains. The opacity both depends on a_1^3 (which decrease slightly) and the degree of condensation f_c (which increases) with the later effect dominating, which leads to a higher final outflow velocity $\langle u \rangle$ of the wind, despite a reduction of the dust absorption per gram of dust.

4.3. Influence of the estimated sticking coefficient

The sticking coefficient (also called the reaction efficiency factor) α enters into the net growth rate of the dust grains

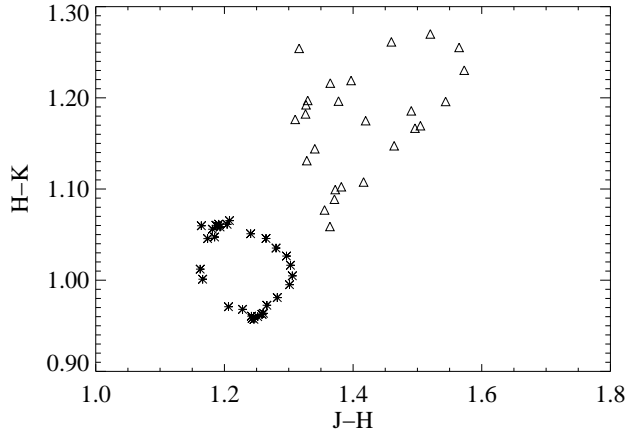


Fig. 5. The colors (J–H) vs. (H–K) for the two models l13drouϱ185 (*) and l13drouϱ185α10 (Δ). The only difference between the two models is the assumed value of the sticking coefficient. The larger the sticking coefficient is assumed to be, the more efficient will the grain formation be and as a consequence the models will look redder when observed in (H–L), (J–H) or (K–L). See Table 4 for details.

(Eq. (5)). However, α is not definitely known as long as we do not know explicitly the sequence of chemical reactions responsible for the dust formation. To demonstrate how uncertainties in the value of α will influence the results of the models we have varied this parameter in otherwise identical models.

In the case of carbon dust formation the most important growth species is expected to be C_2H_2 , but also C, C_2 and C_2H contribute to the growth (Gail & Sedlmayr 1988). In our earlier models we have used the values $\alpha_C = 0.37$, $\alpha_{C_2} = 0.34$, $\alpha_{C_2H} = 0.34$ and $\alpha_{C_2H_2} = 0.34$ to describe the grain growth.

Gail & Sedlmayr (1984) used the value $\alpha_C = 0.3$ adopted from Landolt-Börnstein (1968). Later Gail & Sedlmayr (1988) argued that the sticking coefficient α must be on the order of unity, because it is expected that neutral radical reactions play a dominant role in the formation process of carbon grains. However, if substantial energy barriers are involved in the reactions α may well be less by several orders of magnitude. It is important to remember that if α is small the assumption that nucleation can be treated as a time-independent process will no longer hold. Small values of α should be accompanied by a time-dependent treatment of the dust nucleation (Gail & Sedlmayr 1988).

Salpeter (1973) has shown that the latent heat released when a monomer attaches itself to an N -mer may lead to a small sticking probability if N is small. Thus the sticking coefficient α for clusters with $N \approx N_*$ may be considerably smaller than the sticking coefficient for clusters with $N \gg N_*$. The sticking coefficient is of the order unity for bulk material (Pound 1972).

To test the assumptions for the sticking coefficient we have calculated four models for a star with $L_\star = 13000 L_\odot$, $T_\star = 2700$ K and with the sticking coefficient (α) varying from 0.2 – 1.0 and two cooler models with $L_\star = 10000 L_\odot$ and $T_\star = 2600$ K.

It is clear from Table 4 and Fig. 5 (showing how the colors of two models depend on the chosen value for the sticking coefficient) that using the value of 1 as suggested by Gail & Sedlmayr (1988) compared to our previous values of 0.34–0.37 results in a noticeable reddening of the colors of the stellar model. Fig. 6 shows the mean outflow velocity, the gas density, the gas temperature and the mean degree of condensation for four different phases of the two different models l13drouϱ185α and l13drouϱ185α10. The higher value of the sticking coefficient increases both the degree of condensation and the outflow velocity by about a factor of two. In addition the mass-loss rate increases, leading to a higher optical depth of the circumstellar envelope.

From Fig. 6 it can be seen that dust formation occurs beyond $\approx 2R_\star$ independent of the value assumed for the sticking coefficient since the onset of condensation is determined mainly by the temperature. With the low choice of sticking coefficient only about 10% of the condensable carbon material present in the gas actually condenses into grains, while for the much more favorable choice of sticking coefficient ($\alpha = 1$) twice as much material condenses into grains. A complete condensation of carbon grains is prevented by the rapid velocity increase after the onset of avalanche nucleation and grain growth, and the subsequent rapid dilution of the gas.

4.4. Influence of the surface tension for the dust

In classical homogeneous nucleation theory, the surface tension of the grain material is used to describe the gain of enthalpy by forming a grain out of N monomers in the gas phase.

The surface tension σ_{grain} of amorphous carbon is not known from laboratory experiments, it has therefore become custom to use values for graphite, e.g. one of the values given by Tabak et al. (1975). One problem however is that there are huge variations in the values determined due to the anisotropy of graphite.

As already demonstrated by Tabak et al. (1975), varying the value of the surface tension may produce an enormous change in the nucleation rate. To determine how significant the prescribed value for the surface tension is for our results we have varied it around the value of 1400 erg/cm^2 which was used in previous models (see Table 5).

For the particular model, altering the value of the surface tension of the dust grains by 28% around the value of graphite will make the difference between obtaining mass-loss or not. The value of the surface tension also has a substantial influence on how much of the available material in the circumstellar envelope will condense into

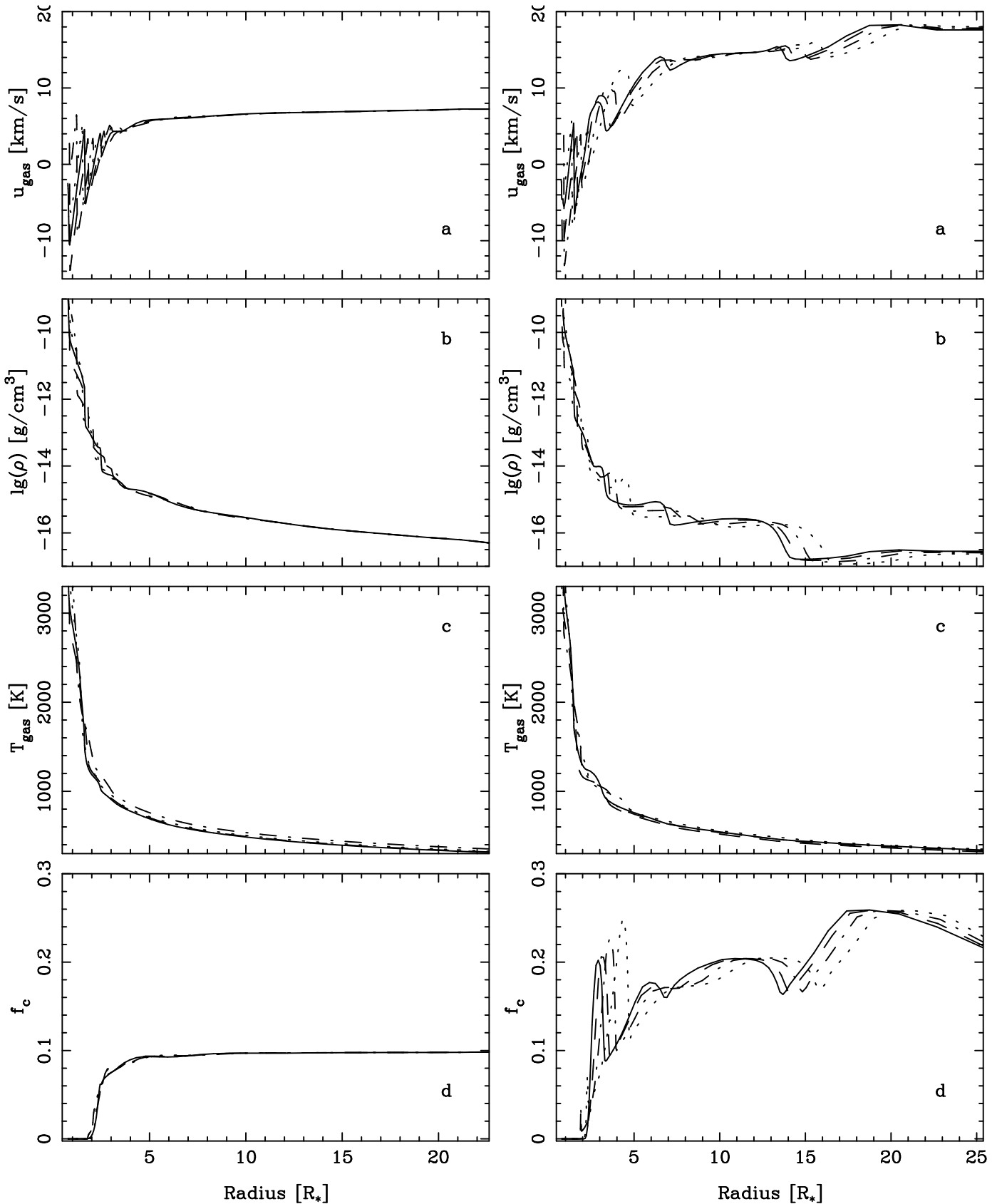


Fig. 6. Models l13drourho185 (left) and l13drourho185alpha10 (right). For four different phases of the two models (a) the outflow velocity of the gas, (b) the gas density, (c) the gas temperature and (d) the degree of condensation is shown. The only difference between the two models is the value used for the sticking coefficient. It is evident that the choice of sticking coefficient has a significant influence on the predicted outflow velocity and the degree of condensation.

Table 5. Influence of the surface tension for the dust formation. *Model parameters:* Same as for model l13drou ρ 185 in Table 2 but with different values for the surface tension σ_{grain} .

Model	σ_{grain} [erg/cm ²]	\dot{M} [M _⊙ /yr]	$\langle u \rangle$ [km/s]	$\langle f_c \rangle$
l13drou ρ 185 σ 10	1000	$8.5 \cdot 10^{-6}$	35	0.76
l13drou ρ 185	1400	$4.9 \cdot 10^{-6}$	7.4	0.10
l13drou ρ 185 σ 18	1800	-	-	-

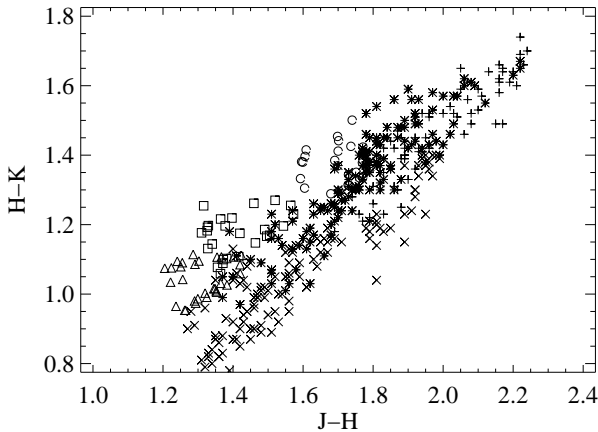


Fig. 7. The colors ($J - H$) vs. ($H - K$) for the three models l13dj10 ρ 199 (\triangle), l13drou ρ 185 α 10 (\square) and l10dj10 ρ 199 (\circ), and three comparable observed carbon Miras R Vol ($+$), R For ($*$), R Lep (\times) (observations from Whitelock et al. 1997).

dust grains. For comparison, the measured surface tension for other materials are: Fe ($\sigma_{\text{grain}} = 1400$ erg/cm²), MgS ($\sigma_{\text{grain}} = 800$ erg/cm²) and SiO ($\sigma_{\text{grain}} = 500$ erg/cm²), see Gail & Sedlmayr (1986).

4.5. Comparison with observations

Near-infrared colors including JHKL³ magnitudes were calculated for a selection of the models. The filter zero points were calculated from a Vega model of Dreiling & Bell (1980), under the assumption that the Vega model has 0.0 mag in all filters.

Whitelock et al. (1997) present JHKL light curves for 11 large-amplitude carbon variables. For a comparison between models and observations we picked the carbon Miras R For, R Lep and R Vol. These stars have moderately thick dust shells and colors comparable with our models (see Fig. 7). According to Olofsson et al. (1993) these stars have outflow velocities of about 16 – 19 km/s. From our set of models we selected those with comparable velocities (see Table 6). We preferred outflow velocities over other

wind properties when selecting the models for this comparison, since this is the most directly observable quantity. The colors on the other hand contain entangled information about the mass-loss rates, the outflow velocities, the degree of condensation, and the optical properties of the grains.

We have not selected the stars for their derived stellar parameters but for their observable wind properties. The observed stars (R For, R Lep and R Vol) and the models (l13drou ρ 185 α 10 and l10dj10 ρ 199) have similar dust mass loss rates and near infrared colors while the gas mass-loss rates for the observed stars and the models differ significantly (see Table 6). We preferred the dust mass-loss rates over the gas mass-loss as a criterion for the comparison since the near IR colors are strongly affected by the dust opacity, as demonstrated by the figures in the preceding section.

The dust mass-loss rates of the observed stars were estimated using the 60 μm IRAS flux. In general there is expected to be a relation between the dust mass-loss rate and the strength of the dust emission. Following Sopka et al. (1985) Olofsson et al. (1993) derive the dust mass-loss rates of these stars using

$$\dot{M}_{\text{dust}} = 2.2 \times 10^{-15} S_{60} v_d D^2 L^{-0.5} M_{\odot} \text{yr}^{-1}, \quad (14)$$

where S_{60} is the IRAS 60 μm flux in Janskys, v_d is the dust expansion velocity in km/s, D is the distance to the source in parsecs and L is the luminosity in units of L_{\odot} . For the dust expansion velocity Olofsson et al. (1993) use two different values, one where the upper limit to the drift velocity is obtained by considering the radiation force on the grains and the drag force due to gas-grain collisions in the limit of supersonic motion. The lower limit for the dust expansion velocity is derived by neglecting drift. As a consequence two different dust mass-loss rates are given by Olofsson et al. (1993), one for the upper limit $\dot{M}_{\text{dust}}^{\text{upper}}$ and one for the lower limit $\dot{M}_{\text{dust}}^{\text{lower}}$.

The gas mass-loss rates of the observed stars given in Table 6 were derived by Olofsson et al. (1993) based on observed CO emission using equation (5) of Knapp & Morris (1985) which has the form

$$\dot{M}_{\text{gas}} = \left(1 + \frac{4n_{\text{He}}}{n_{\text{H}}} \right) \frac{T_{\text{mb}} v_e^2 D^2}{A(B, J) f_{\text{CO}}^{0.85}} M_{\odot} \text{yr}^{-1}, \quad (15)$$

where $n_{\text{He}/\text{H}}$ is the total number density of Helium/Hydrogen, T_{mb} is the main-beam brightness temperature, v_e represent the gas expansion velocities, D is the distance to the source, $A(B, J)$ is a quantity that depends on the beam size used, B , and the transition observed, $J \rightarrow J - 1$, and f_{CO} is the abundance of CO with respect to H₂. Schöier & Olofsson (2001) find that the gas mass-loss rates resulting from Eq. (15) are systematically underestimated compared to a more detailed radiative transfer analysis (see their Fig. 8), however, for these particular stars the values agree reasonable well.

In the models discussed here we obtain higher gas-to-dust ratios than the values given by Olofsson et al. (1993).

³ Central filter wavelength [μm]: J = 1.22, H = 1.63, K = 2.19, L = 3.45.

Table 6. Data for three observed carbon-rich Mira’s with similar colors and outflow velocities as the calculated models (Tables 2 and 4). The observed velocities and mass-loss rates are from Olofsson et al. (1993).

Star	Period [days]	v_{out} [km/s]	M_{gas} [M_{\odot}/yr]	$M_{\text{dust}}^{\text{lower}}$ [M_{\odot}/yr]	$M_{\text{dust}}^{\text{upper}}$ [M_{\odot}/yr]	Symbol in Fig. 7
R For	389	16.3	1.0×10^{-6}	2.4×10^{-9}	3.5×10^{-9}	*
R Lep	427	17.0	7.0×10^{-7}	1.9×10^{-9}	2.8×10^{-9}	×
R Vol	454	18.5	2.5×10^{-6}	4.2×10^{-9}	5.1×10^{-9}	+
Model	Period [days]	$\langle u \rangle$ [km/s]	M_{gas} [M_{\odot}/yr]	M_{dust} [M_{\odot}/yr]		Symbol in Fig. 7
l13dj10 ρ 199	650	15	5.6×10^{-6}	6.3×10^{-10}		\triangle
l13drou ρ 185 α 10	650	17	7.0×10^{-6}	3.5×10^{-9}		\square
l10dj10 ρ 199	650	16	7.0×10^{-6}	3.5×10^{-9}		\circ

This could be a consequence of the fact that some of the stellar parameters differ from these of the models. As mentioned above, the models and stars for the comparison were chosen for similar wind velocities and dust mass-loss rates, not for comparable stellar parameters. In this sense, we are rather comparing the observable properties of the circumstellar dust shells than of the stars and their surrounding gas envelopes. Therefore, the comparison shown here should not be considered as an attempt to fit observations of individual stars but to investigate certain wind properties of our models.

While the average colors of the models are comparable to the average colors of the observed stars, see Fig. 7, the temporal variation of the colors for a given model is smaller than the variations observed in the individual stars. This is probably a consequence of relatively small bolometric luminosity variations in the models.

Figure 7 shows a comparison of models and observed stars for the colors J-H vs. H-K. A qualitatively similar relation between models and observations is obtained for the colors K-L vs. H-K.

5. Conclusions

We have investigated in detail how the predicted wind properties of carbon-rich AGB stars are influenced by the choice of micro-physical dust parameters i.e. the optical properties of the dust, the intrinsic dust density, the assumed sticking coefficients and the surface tension of the grain material (these two last parameters control the efficiency of the dust formation).

For the theoretical predictions of mass-loss it is important to know how the uncertainty in the chosen dust parameters affects the obtained results. Varying the micro-physical parameters within the range typical of possible materials can change the value for the mean outflow velocity of the gas and dust as well as the predicted degree of dust condensation by a factor of ten and the predicted mass-loss by a factor of four. In the transition region between models with and without mass-loss the choice of micro-physical parameters is vital for whether a particu-

lar set of stellar parameters will give rise to a dust-driven mass-loss or not.

The main source of momentum for the stellar wind is the radiation pressure on dust. The radiation pressure on the dust and the radiative equilibrium grain temperature is determined by the wavelength dependence of the grain extinction efficiency. The steeper the dependence of wavelength, the larger the difference between the equilibrium grain temperature and the radiation temperature. The radiation pressure on the other hand is proportional to the flux mean opacity which both depends on the slope of the extinction efficiency as a function of wavelength and on its absolute value. The latter may differ by almost an order of magnitude for different types of amorphous carbon in the critical region around $1 \mu\text{m}$. The density of the grain material has to be chosen consistently with the grain extinction efficiency.

The surface tension of the grain material and the sticking coefficients are very significant for the calculated rates at which grains are formed out of the gas (nucleation) and at which new material is added to existing grains (grain growth). Even a moderate variation of the values within the range expected for possible materials has noticeable consequences for the properties of the dust-driven stellar winds, including the resulting near-infrared colors.

The colors are similar to stars with comparable dust mass-loss rates and outflow velocities, however, we have not attempted to fit any individual stars.

Acknowledgements. The authors would like to thank Kjell Eriksson for valuable discussions. ACA gratefully acknowledges support from the Carlsberg Foundation. This work was supported by NorFA, the Swedish Research Council (VR) and the Royal Swedish Academy of Sciences (KVA).

References

- Allen C.W., 1973, *Astrophysical Quantities*, The Athlone Press, London
- Andersen A., Loidl R. & Höfner S., 1999, *A&A* 349, 243
- Becker R. & Döring W., *Ann. Physik*, A125, 719

- Bohren C.F. & Huffman D.R., 1983, *Absorption and Scattering of Light by Small Particles* (John Wiley & Sons, New York)
- Bussoletti E., Colangeli L., Borghesi A. & Orofino V., 1987, *A&AS* 70, 257
- Campbell M.F., Harvey P.M., Hoffmann W.F., et al., 1976, *ApJ* 208, 396
- Donn B. & Nuth J.A.III., 1985, *ApJ* 288 187
- Dorfi E. & Feuchtinger M., 1995, *Computer Physics Communications* 89, 69
- Dorfi E.A. & Höfner S., 1991, *A&A* 248, 105
- Draine B.T. & Lee H.M., 1984, *ApJ* 285, 89
- Dreiling L.A. & Bell R.A., 1980, *ApJ* 241, 736
- Feder J., Russel K.C., Lothe J. & Pound G.M., 1966, *Advances in Physics* 15, 111
- Fleischer A.J., Gauger A. & Sedlmayr E., 1992, *A&A* 266, 321
- Gail H.-P. & Sedlmayr E., 1984, *A&A* 132, 163
- Gail H.-P. & Sedlmayr E., 1986, *A&A* 166, 225
- Gail H.-P. & Sedlmayr E., 1987a, *A&A* 171, 197
- Gail H.-P. & Sedlmayr E., 1987b, *A&A* 177, 186
- Gail H.-P. & Sedlmayr E., 1988, *A&A* 206, 153
- Gauger A., Gail H.-P. & Sedlmayr E., 1990, *A&A* 235, 345
- Gürtler J., Kömpe C. & Henning Th., 1996, *A&A* 305, 878
- Hale B.N., 1986, *Phys. Rev. A* 33, 4156
- Hale B.N., Kemper P. & Nuth J.A.III., 1989, *J. Chem. Phys.* 91, 4314
- Höfner S., 1999, *A&A* 346, L9
- Höfner S. & Dorfi E.A., 1992, *A&A* 265, 207
- Höfner S. & Dorfi E.A., 1997, *A&A* 319, 648
- Höfner S., Feuchtinger M.U. & Dorfi E.A., 1995, *A&A* 279, 815
- Höfner S., Gautschy-Loidl R., Aringer B. & Jørgensen U.G., 2002, *A&A* in press
- Huffmann D.R., 1988, in *Experiments on Cosmic Dust Analogues*, Kluwer Academic Publishers, eds. E. Bussoletti, C. Fusco, G. Longo, 25
- Jäger C., Mutschke H. & Henning Th., 1998, *A&A* 332, 291
- Jura M., 1987, *ApJ* 313, 743
- Jørgensen U.G., 1997, In: van Dishoeck E.F. (ed.) *Molecules in Astrophysics: Probes and processes*, [Kluwer], IAU Symp. 178, 441
- Knapp G.R. & Morris M., 1985, *ApJ* 292, 640
- Landolt-Börnstein, 1968, *Zahlenwerte und Funktionen*, vol. 5b, Springer Verlag, Berlin
- Martin P.G. & Rogers C., 1987, *ApJ* 322, 374
- Martinez D.M., Ferguson F.T., Heist R.H. & Nuth J.A.III., 2001, *J. Chem. Phys.* 115, 310
- Maron N., 1990, *Ap&SS* 172, 21
- Nuth J.A. & Ferguson F., 1993, *Ceramic Transactions* 30, 23
- Olofsson H., Eriksson K., Gustafsson B. & Carlström U., 1993, *ApJS* 87, 267
- Pound G.M., 1972, *J. Phys. Chem. Ref. Data* 1, 135
- Rouleau F. & Martin P.G., 1991, *ApJ* 377, 526
- Salpeter E.E., 1973, *J. Chem. Phys.* 58, 4331
- Schöier F.L. & Olofsson H., 2001, *A&A* 368, 969
- Sedlmayr E., 1994, in *Molecules in the Stellar Environment*, LNP 428, ed. U.G. Jørgensen (Springer, Berlin), 163
- Sopka R.J., Hildebrand R.H., Jaffe D.T., et al., 1985, *ApJ* 294, 242
- Stull D.R. & Prophet H., 1971, *JANAF Thermochemical Tables*, 2nd Ed., Nat. Bureau of Standards, Washington, (NSRDS-NBS37)
- Tabak R.G., Hirth J.P., Meyrick G. & Roark T.P., 1975, *ApJ* 196, 457
- Whitelock P., Feast M., Marang F. & Overbeek M., 1997, *MNRAS* 288, 512